scientific reports

Check for updates

OPEN

Huangqin decoction disrupts energy metabolism of *Trichophyton rubrum*, with isocitrate lyase as a potential target

Suqing Yang[1], Yican He[2], Youjin Ge[3], Baode Shen[4] & Chengying Shen[1]✉

The dermatophyte *Trichophyton rubrum* (*T. rubrum*) is a highly specialized filamentous fungus that primarily infects keratinized tissues and is the most common pathogen isolated from human dermatophytosis. Huangqin decoction (HQD), a classical traditional Chinese medicine (TCM) formula, has been shown to exhibit inhibitory effects against *T. rubrum* in our previous study. However, the underlying mechanisms responsible for these effects remain poorly understood. This study aimed to elucidate the comprehensive mode of action of Huangqin decoction (HQD) against *T. rubrum* as a whole by integrating transcriptome sequencing validated by quantitative real-time PCR (qRT-PCR) and enzymatic activity assays. By treating *T. rubrum* with HQD at minimum inhibitory concentration (MIC), a total of 338 differentially expressed genes (DEGs) were detected in *T. rubrum* after HQD exposure (q-value < 0.05). Gene function and Encyclopedia of Genes and Genomes (KEGG) enrichment analyses indicated that DEGs were significantly related to energy metabolism. The expression levels of six DEGs by the involvement of energy metabolism, including the degradation of branched-chain amino acids and the glyoxylate cycle, were verified by qRT-PCR. Three key enzymes in the glyoxylate cycle were further examined by enzymatic activity assays. The results showed that compared to the control group, activities of citrate synthase (CS), aconitate hydratase (ACO), and isocitrate lyase (ICL) in *T. rubrum* were predominantly affected by HQD (p-value < 0.05). The overall evidence suggested that the interference with energy metabolism contributed to the mode of action of HQD against *T. rubrum*. Given that the glyoxylate cycle represents an important specific metabolic process in fungi, and the involved enzyme ICL is absent in humans, ICL emerges as a potential antifungal target of HQD against *T. rubrum*. In summary, our study provides a theoretical basis for the mechanisms of HQD upon *T. rubrum* infections and makes contributions to the clinical application of HQD against fungi.

Keywords Huangqin decoction, *Trichophyton rubrum*, Dermatomycosis, Energy metabolism, The glyoxylate cycle, Isocitrate lyase

Abbreviations

T. rubrum	*Trichophyton rubrum*
HQD	Huangqin decoction
TCM	Traditional Chinese medicine
MIC	Minimal inhibitory concentration
DEGs	Differentially expressed genes
KEGG	Kyoto Encyclopedia of Genes and Genomes
COG	Clusters of Orthologous genes
GO	Gene ontology
qRT-PCR	quantitative real-time PCR
CS	Citrate synthase
ACO	Aconitate hydratase

[1]Department of Pharmacy, Jiangxi Provincial People's Hospital, The First Affiliated Hospital of Nanchang Medical College, Nanchang, P.R. China. [2]School of Pharmacy, Chengdu University of Traditional Chinese Medicine, Chengdu, P.R. China. [3]Center for Drug Clinical Trials, Nanchang People's Hospital (The Third Hospital of Nanchang), Nanchang, P.R. China. [4]Key Laboratory of Modern Preparation of Traditional Chinese Medicine, Ministry of Education, Jiangxi University of Chinese Medicine, Nanchang, P.R. China. ✉email: 984075899@qq.com

ICL	Isocitrate lyase
SDB	Sabouraud dextrose broth
SDA	Sabouraud Dextrose Agar
BP	Biological process
CC	Cellular component
MF	Molecular function
DBT	dihydrolipoyl transacylase
OXCT	3-oxoacid CoA-transferase
HMGCL	hydroxymethylglutaryl-CoA lyase
TCA cycle	the tricarboxylic acid cycle

Dermatomycosis, a fungal infection that exclusively grows in keratinized host structures, is reported to affect about 20–25% of the world's population, and that of the hair, skin, or nails is one of the most common fungal infections worldwide[1–4]. In geographic regions with high prevalence, the incidence of dermatomycosis reaches as high as 40–60%[5–7]. Dermatomycosis is difficult to cure and is prone to recurrence and reinfection, which seriously affects the quality of patients' lives and has significant economic implications. What's more important, the infection can progress from a localized disease to an invasive infection when the host's immune system is weakened by various factors[8,9]. The clinically predominant dermatophyte species causing skin infections is *Trichophyton rubrum* (*T. rubrum*), accounting for approximately 80% of dermatomycosis cases[10]. Clinical drugs commonly used to treat infections were the azole class, triazoles, heterocyclic benzofurans, and allylamines. However, due to the prolonged therapy duration, limited efficacy, emerging antifungal resistance, and adverse effects of available drugs, the clinical treatment of these infections remains challenging[11,12].

In recent years, traditional Chinese medicine (TCM) has emerged as a valuable type of complementary and alternative medicine for the treatment of dermatomycosis, due to its broad-spectrum antifungal activity, low incidence of drug resistance, and relatively mild toxicity[13–15]. TCM is one of the oldest medical systems in the world and has proven to be both safe and effective. Huangqin decoction (HQD), a classical TCM formula from *Shang Han Lun* written by Zhang Zhongjing in the Han dynasty, is an aqueous extract of four herbal materials, including the roots of *Scutellaria baicalensis* Georgi, *Paeonia lactiflora* Pall., *Glycyrrhiza uralensis* Fisch, and the fruit of *Ziziphus jujuba* Mill. Modern research has demonstrated that HQD could exhibit anti-inflammatory effects[16,17] and antifungal properties[18]. The principal bioactive components of HQD possess diverse pharmacological activities. For example, paeoniflorin[19] has anti-inflammatory and immunomodulatory effects. Glycyrrhizin[20,21] has antimicrobial properties. Baicalin[22], baicalein[23] and wogonin[23] have antifungal activities. Our previous research demonstrated that HQD could significantly inhibit the growth of *T. rubrum*, with a minimal inhibitory concentration (MIC) of 3.13 mg/mL[24]. However, the study utilized several reagents that focus on common enzymes such as squalene epoxidase (SE), sterol 14α-demethylase P450 (CYP51), malate dehydrogenase (MDH), etc., to investigate whether these enzymes in *T. rubrum* would be affected by HQD. The comprehensive mode of action of HQD against *T. rubrum* remains unclear.

The transcriptome is the entire set of RNA transcripts from a particular tissue, including messenger RNA, regulating the transmission of genetic information from DNA to protein[25–27]. Transcriptome sequencing can simultaneously detect and quantify almost all transcripts in a species at specific developmental stages or physiological states. The results can display the involvement of differentially expressed genes (DEGs) between healthy and diseased groups, across biological samples with or without drug treatment, which provides an opportunity to elucidate the underlying molecular mechanisms of diseases or drugs at the transcriptome level[28–32]. In recent years, due to the high throughput and high sensitivity, transcriptome sequencing has made tremendous progress in exploring the mode of action of medicines against fungi or bacteria[33–35].

In the present study, we elucidated the preliminary mechanisms of HQD against *T. rubrum* through combining transcriptome sequencing verified by quantitative real-time PCR (qRT-PCR) and enzymatic activity assays, aimed to provide new insights into the therapeutic intervention against dermatophytes. Technically, *T. rubrum* strains were treated with HQD at a concentration of MIC, and then transcriptome sequencing was performed to identify DGEs in *T. rubrum* after HQD exposure. Gene function analysis and Kyoto Encyclopedia of Genes and Genomes (KEGG) enrichment analysis were conducted to reveal the functions and signaling pathways regulated by these DEGs. The transcriptome findings were further validated by qRT-PCR for DEGs of particular interest. Finally, enzymatic activity assays were conducted to explore the potential molecular targets of HQD against *T. rubrum*.

Materials and methods

Materials

The HQD formula consists of four medical herbs: the roots of *Scutellaria baicalensis Georgi* (skullcap), *Paeonia lactiflora Pall.* (peony), *Glycyrrhiza uralensis Fisch.* (licorice), and the fruit of *Ziziphus jujuba Mill.* (jujube), in a ratio of 3:2:2:2, respectively. All herbal materials were purchased from Jiangxi Peng's Guoyaotang Sliced Herb Co., Ltd. and authenticated by Chief Pharmacist Ping Ying from the Department of Pharmacy, Jiangxi Provincial People's Hospital (the First Affiliated Hospital of Nanchang Medical College), PR China. A filamentous fungus total protein extraction kit was purchased from Beibo Biotechnology Co., Ltd. Aconitate hydratase (ACO) reagent kit was obtained from Shanghai MLBIO Biotechnology Co., Ltd. Citrate synthase (CS) and isocitrate lyase (ICL) reagent kits were bought from Solarbio Co., Ltd.

Preparation of HQD

The preparation of HQD was conducted as previously described in our earlier study[36]. According to the prescription of HQD, 18 g of skullcap, 12 g of peony, 12 g of licorice, and 12 g of jujube were soaked together in

distilled water (1:10, w/v) for 30 min and then decocted for 1 h. After filtration, the residue was boiled in distilled water (1:8, w/v) for another 1 h. The two filtrates were combined, concentrated under reduced pressure at 60 ℃, and freeze-dried at room temperature to obtain 21.25 ± 1.01 g of lyophilized powder.

Fungal strains and HQD treatment

The fungal strain of *T. rubrum* STRB12 was provided by researcher Ping Zhan, co-author of the reference[37]. The strain was identified through phenotype characterization, microscopic analysis, and internal transcribed spacer (ITS) sequence comparison[37]. Prior to experiments, the fungal strains were reactivated and subcultured twice on the Sabouraud Dextrose Agar (SDA: 15 g/L agar, 40 g/L glucose, 10 g/L peptone, 0.125 g/L chloromycetin) to purify the colony and enhance its vitality. Thereafter, *T. rubrum* was inoculated into SDA and incubated at 28 ± 2 °C for 7–14 days, and spores were harvested from sporulating colonies and suspended in a sterile 0.85% NaCl solution containing 1% Tween-20. The spore concentrations were determined and adjusted to the inoculum of 5.0×10^5 CFU/mL using a hemocytometer. The working suspension with a final inoculum of 5.0×10^3 CFU/mL was prepared by 100-fold dilution of the inoculum suspension with Sabouraud dextrose broth (SDB: 40 g/L glucose, 10 g/L peptone, 0.125 g/L chloromycetin).

The experimental strain samples were divided into two groups: (1) the HQD-treatment group: three biological replicates (STRB12-HQD1, STRB12-HQD2, STRB12-HQD3) exposed to HQD at the MIC (i.e., 3.13 mg/mL[24]), a stress concentration to elicit the antifungal response in *T. rubrum*; (2) the control group: three replicates (STRB12-KB1, STRB12-KB2, STRB12-KB3) treated with an equal volume of SDB. After 5 days of incubation at 28 °C, the mycelia were harvested by sterile Whatman paper, washed twice with sterile distilled water, and dried on filter paper for RNA extraction.

Transcriptome sequencing

RNA extraction and library construction for sequencing

Total RNA was isolated from the tissues using Trizol (Invitrogen, Carlsbad, CA, USA) following the manufacturer's instructions and the protocol described in reference[34]. RNA concentration was measured using a Qubit 4.0 fluorometer, while RNA integrity was assessed with an Agilent Bioanalyzer 2100 system (Agilent Technologies, MA, USA), and RNA purity was determined using a NanoDrop 2000 (Thermo Fisher Scientific, MA, USA). After the total RNA passed quality control, Oligo(dT)-attached magnetic beads were used to purify the eukaryotic messenger RNA (mRNA). Purified mRNA was fragmented into short fragments with RNA fragmentation buffer. Using fragmented mRNA as a template, the first-strand complementary DNA (cDNA) was generated using random hexamer-primed reverse transcription, followed by a second-strand cDNA synthesis. Hieff NGS® DNA Selection Beads were used to purify double-stranded products and perform fragment selection. Finally, PCR amplification was performed to obtain the final library. After the library was qualified, the DNBSEQ-T7 was used for paired-end sequencing.

Sequencing data analysis

The sequencing data were filtered with SOAPnuke (v1.5.2)[38] by removing reads containing adapters and poly-N sequences, as well as low-quality reads or those with uncertain bases, to obtain clean reads. Meanwhile, the quality metrics of the clean data, including Q20, Q30, GC-content, and the sequence duplication level, were determined. Finally, the clean reads were aligned to the reference genome sequence (GenBank assembly of GCA_000151425.1, species of *Trichophyton rubrum* CBS 118892, genome size of 22.5 Mb) using the Hisat2 (v2.0.4)[39] tools. Data from all the sequencing are deposited in the NCBI Gene Expression Omnibus (GEO) database[40] under the accession number GSE300994.

Detection of differentially expressed genes

The expression level for each gene was quantified using the FPKM (Fragments per kilobase of transcript per million fragments mapped) method implemented in StringTie (v2.1.2)[41]. The differences of gene expression profiles between the HQD-treatment group and the control group were calculated and compared by the DESeq2 R package (v1.4.5)[42]. The statistical *p*-values across the two groups were adjusted using the Benjamini-Hochberg method to control the false discovery rate (FDR)[43]. A cut-off threshold of $|\log2(\text{fold change})|$ ($|\log2(FC)|$) ≥ 1 and FDR-adjusted *p*-value (also called *q*-value) < 0.05 was applied to define up-regulated and down-regulated transcripts. Visualization of the information on the differentially expressed genes (DEGs) was performed by the R package (v3.6.1), including a volcano plot, a correlation plot, a bar plot, and a cluster heatmap.

Gene function analysis and KEGG pathway enrichment analysis

Gene function analysis was conducted to ascertain the potential functions of total DEGs, ranging from cellular processes to organismal functions and ecosystem interactions. In this study, the Clusters of Orthologous Genes (COG) analysis and Gene Ontology (GO) analysis were performed based on the homologous classification of gene products in the COG database[44] and ontologies of gene products in the GO database[45], respectively. Pathway classification analysis was conducted to identify high-level functions and utilities of the biological system, such as metabolic pathways or signaling transduction pathways, using the KEGG database[46–48]. The KEGG pathway enrichment of the DEGs was performed using KOBAS software (v3.0)[49], and pathways with a statistical *q*-value < 0.05 were assigned as significantly enriched.

The qRT-PCR validation

The expression levels of six DEGs in *T. rubrum* affected by HQD, as identified in the transcriptome sequencing results, were further verified by qRT-PCR. Fungal suspension preparation and HQD treatment followed the protocol described in the 'Fungal strains and HQD treatment' section. Three independent fungal samples from

both the HQD-treatment group and the control group were used for qRT-PCR analysis. Technically, 1 μL of total RNA from each sample was reverse-transcribed into first-strand cDNA using SynScript® III RT SuperMix according to the manufacturer's instructions. The cDNA was diluted 3-fold as a qPCR template. Quantitative RT-PCR experiments were performed using the ABI QuantStudio StepOne Plus system with ArtiCanCEO SYBR qPCR Mix according to the manufacturer's protocol. The thermal cycling conditions were initial denaturation at 95 °C for 5 min, followed by 40 cycles of 94 °C for 15 s, 60 °C for 20 s, and 72 °C for 20 s for annealing, and then an extension. For each test gene, the reactions were performed in triplicate.

The $2^{-\Delta\Delta Ct}$ method[50] was used to quantify the relative expression level of each gene, with 18 S rRNA as the endogenous control. The primers for the examined genes were listed in Table 1. Statistical difference across groups was analyzed by Multiple t-tests using GraphPad Prism software (v6.01), and the results for each gene were presented as the mean ± standard deviations. Genes with a p-value < 0.05 were considered significantly differentially expressed.

Enzyme activity assays

The enzyme activities of three key enzymes involved in the glyoxylate cycle, including citrate synthase (CS), aconitate hydratase (ACO), and isocitrate lyase (ICL), were further identified. Fungal suspension preparation and HQD treatment followed the protocol described in the 'Fungal strains and HQD treatment' section. Mitochondria were isolated from *T. rubrum* mycelia for the activity assays of ACO and CS. Approximately 0.05 g of wet mycelia was weighed, and the corresponding reagents were added to prepare the homogenization. The homogenization medium was centrifuged at 600 g for 5 min at 4 °C to remove the cell debris and unbroken cells. The supernatant was collected and centrifuged at 11 000 g for 10 min at 4 °C. The resulting pellet was collected as the mitochondria fraction, resuspended in the corresponding reagents, and used for measuring protein concentrations and enzymatic activities. For the ICL enzyme activity assay, the working solution and reagents were strictly configured according to the kit instructions. Approximately 0.05 g of wet mycelia was weighed, and 1 mL of the extract reagent was added to prepare the homogenization. The homogenization medium was centrifuged at 15 000 g for 20 min at 4 °C. The supernatant was collected as the sample for testing, mixed with the working solution and corresponding reagents, and used for measuring protein concentrations and enzymatic activities.

The activities of ICL, ACO, and CS were measured in strict accordance with the protocols provided in their respective reagent kits. Each experiment was repeated three times to ensure reproducibility. The activities of ICL and CS were reported in U mg^{-1} protein, and that of ACO was expressed as nmol min^{-1} mg^{-1} protein. Statistical differences between the HQD-treatment group and the control group were assessed using a Multiple t-test using GraphPad Prism software (v6.01).

Results

Sequencing data quality and alignment statistics

The fungal samples subjected to transcriptome sequencing were divided into two groups: the HQD-treatment group and the control group, with three biological replicates for each group. Across these six samples, a total of 41.79 GB of clean data was generated. Following the alignment of the clean reads to the reference genome, the mapped reads were found to range from 88.52% to 98.07%. Additionally, the average proportion of Q30 across all six samples exceeded 95.31%. These results collectively confirm that the sequencing data were of high quality and met the requirements for subsequent analyses, as presented in Table 2.

Gene ID	Gene Product	Primer	Sequences (5'–3')	Product size (bp)
-	18 S rRNA	F	CGCTGGCTTCTTAGAGGGACTAT	51
		R	TGCCTCAAACTTCCATCGACTT	
TERG_01272	CS	F	GCACGGCAAGGTACGAATTATATG	128
		R	ACCGTAGTGGTGGAAGAGGA	
TERG_01076	ACO	F	GAATACGACTCCGTCCCTGC	181
		R	GGTTGGTCTCGTGGATACGG	
TERG_01271	ICL	F	ACTTGGTGCAGAAACGCGAA	172
		R	ATCGAGAGCTATCATGACTTACGG	
TERG_07318	DBT	F	TCGGCATTGGCAAGATCAGA	166
		R	GCATCTGGGTTCTCGACCAT	
TERG_01052	OXCT	F	AGTGTATTCTTTCTGCCTCTTCC	143
		R	GCAGTAGGGTTGGAGACGAG	
TERG_03476	HMGCL	F	AGGGTGCCCGTACTCTAAGG	165
		R	CCGGCTCTGCTATCGTTCTC	

Table 1. The primers of examined genes applied in qRT-PCR assay. **Abbreviations**: CS, citrate synthase; ACO, aconitate hydratase; ICL, isocitrate lyase; DBT, dihydrolipoyl transacylase; OXCT, 3-oxoacid CoA-transferase; HMGCL, hydroxymethylglutaryl-CoA lyase.

Sample	Clean read	GC Content	%≥Q30
STRB12-HQD1	23,258,838	52.70%	95.39%
STRB12-HQD2	23,332,718	52.45%	96.48%
STRB12-HQD3	23,251,078	52.24%	96.64%
STRB12-KB1	23,034,478	52.42%	95.31%
STRB12-KB2	23,264,579	52.28%	96.55%
STRB12-KB3	23,176,289	52.22%	96.45%

Table 2. The quality control statistics of sequencing data.

Differential expression genes in *T. rubrum* after HQD exposure

To identify DEGs in *T. rubrum* in response to HQD, the gene expression levels in *T. rubrum* were compared between the HQD-treatment group and the control group. As visualized by the volcano plot, correlation plot, and bar plot in Fig. 1, a total of 338 genes in *T. rubrum* exhibited significant expression changes after HQD exposure (q-value < 0.05), of which 199 genes were up-regulated, and 139 genes were down-regulated. Hierarchical clustering analysis was performed on these DEGs, and results from the cluster heatmap in Fig. 1 revealed that expression profiles of DEGs were similar within the same group but distinct between different groups. This observation indicated that the sample repeatability was good and that HQD effectively modulates the gene expression profiles of *T. rubrum*. These DEGs serve as the key to exploring the antifungal mechanism of HQD against this pathogen.

Functional analysis of DEGs in *T. rubrum* in response to HQD

To investigate the biological functions in *T. rubrum* potentially affected by HQD, a total of 338 DEGs were mapped into the COG and GO databases. Through COG annotation, COG functional categories were predominantly recognized as "carbohydrate transport and metabolism" and "energy production and conversion", as shown in Fig. 2A. Through GO annotation, DEGs were annotated from 3 perspectives: biological process (BP), cellular component (CC), and molecular function (MF), as shown in Fig. 2B. Specifically, in the BP category, DEGs were enriched in "metabolic process" and "cellular process". In the CC category, the "membrane", "membrane part", and "cell" demonstrated the most significant enrichment of DEGs. In the MF category, DEGs were abundant in "catalytic activity" and "binding". Detailed information on expression values and gene annotations for the DEGs is provided in the Additional file 1.

The KEGG enrichment results revealed that DEGs were enriched in 47 signaling pathways, with the top 20 pathways visualized in Fig. 3. Notably, the most prominent DEGs were highly enriched (q-value < 0.05) in 6 pathways, which are listed in ascending order of q-value as follows: "valine, leucine and isoleucine degradation", "indole alkaloid biosynthesis", "ABC transporters", "synthesis and degradation of ketone bodies", "starch and sucrose metabolism", and "glyoxylate and dicarboxylate metabolism". Among these six pathways, three were identified as being closely related to energy metabolism, namely "valine, leucine and isoleucine degradation", "synthesis and degradation of ketone bodies", and "glyoxylate and dicarboxylate metabolism". This finding was aligned with the enrichment of DEGs in GO terms related to "metabolic process" and "catalytic activity," as well as the predominance of COG functional categories in "carbohydrate transport and metabolism" and "energy production and conversion". Detailed information on the enriched pathways of DEGs is provided in the Additional file 2.

Exposure to HQD resulted in significant down-regulation of all DEGs in these three pathways (q-value < 0.05), as indicated by the pathway-associated circles in Fig. 3. As shown in Fig. 4, the 11 affected DEGs encoded key metabolic enzymes, including citrate synthase (TERG_01272, CS), aconitate hydratase (TERG_01076, ACO), isocitrate lyase (TERG_01271, ICL), dihydrolipoyl transacylase (TERG_07318, DBT), 3-oxoacid CoA-transferase (TERG_01052, OXCT), hydroxymethylglutaryl-CoA lyase (TERG_03476, HMGCL), acetyl-CoA acetyltransferase (TERG_01051, ACAT), and four additional genes (TERG_02836, TERG_04293, TERG_04294, and TERG_06712).

qRT-PCR validation of DEGs in *T. rubrum*

To validate the transcriptome sequencing results, six DEGs from the above genes were chosen for expression verification by qRT-PCR assay using independent fungal samples in the presence or absence of HQD. These DEGs were functionally associated with energy metabolism, including three involved in leucine degradation (DBT, ACAT, and HMGCL) and three in the glyoxylate cycle (CS, ACO, and ICL). Detailed information on these DEGs is provided in Table 3.

Each sample gene (including the reference gene) exhibited a single, sharp, and reproducible peak in its melting curve in both the HQD-treated and control groups, with no additional peaks or broad signals indicative of non-specific amplification or primer dimers, as depicted in the Additional Fig. 1. Technical replicates for each gene showed highly concordant melting temperatures (T_m), ranging from ~ 80 °C to ~ 87 °C. These results confirmed the specificity and reproducibility of the qRT-PCR assays and the reliability of our gene expression data.

As shown in Fig. 5A, after HQD treatment, the expression levels of DBT, OXCT, HMGCL, CS, ACO, and ICL were predominantly downregulated in *T. rubrum* (p-value < 0.05). The qRT-PCR results demonstrated that the expression patterns of the selected DEGs highly matched those of the FPKM values derived from transcriptome sequencing under identical treatment conditions. This consistency confirms the reliability of the transcriptome

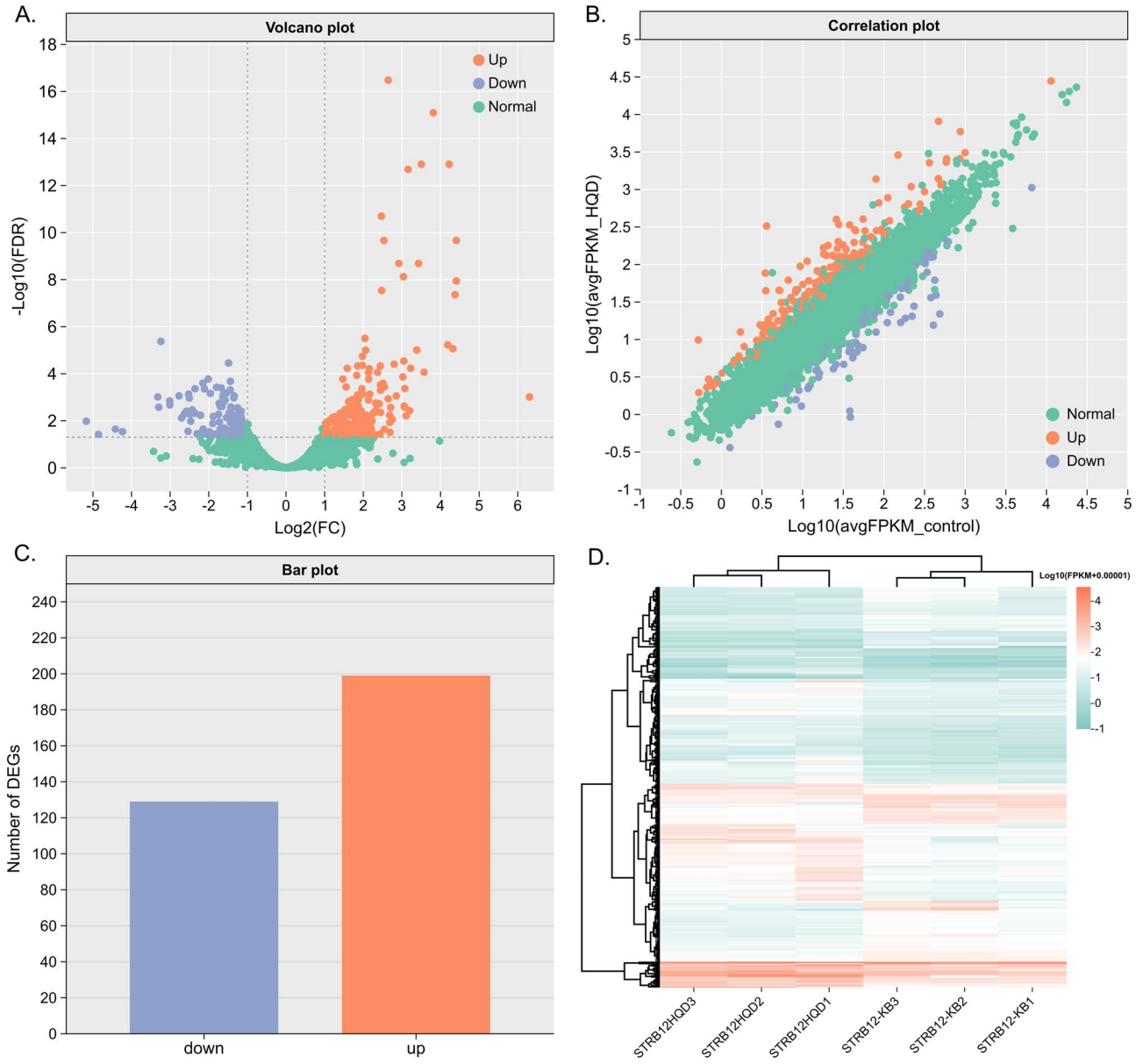

Fig. 1. Differentially expressed genes in *T. rubrum* affected by HQD. In the volcano plot (**A**) and correlation plot (**B**), blue dots represent down-regulated DEGs, orange dots refer to up-regulated DEGs, and green dots indicate non-DEGs. In the bar plot (**C**), the blue and orange bars display the number of down- and up-regulated DEGs, respectively. In the cluster heat map (**D**), each row is a DEG.

sequencing data and further supports the conclusion that HQD interfered with the energy metabolism of *T. rubrum*.

Effects of HQD on enzymes involved in the glyoxylate cycle of *T. rubrum*

Given that the glyoxylate cycle represents an important specific metabolic process in fungi and is absent in humans, three enzymes involved in the cycle – CS, ACO, and ICL – were further investigated by considering their potential as antifungal targets. The enzymatic activities of these enzymes were measured in *T. rubrum* mycelia from both HQD-treatment and control groups. Specifically, ICL activity was assayed in mycelial extracts, whereas CS and ACO activities were determined in the mitochondrial fractions. The results demonstrated that exposure to HQD significantly reduced the activities of CS, ACO, and ICL in *T. rubrum* (p-value < 0.05). As shown in Fig. 5B, in the absence of HQD treatment, the activities of CS, ACO, and ICL reached 117.36 ± 13.29 U mg^{-1}, 12.22 ± 1.98 nmol min^{-1} mg^{-1}, and 9.73 ± 0.70 U mg^{-1} protein, respectively, which were significantly higher than those in the HQD-treated group (p-value < 0.05). When *T. rubrum* was treated with HQD at MIC, the activities of CS, ACO, and ICL in *T. rubrum* were reduced to 32.75 ± 4.60 U mg^{-1}, 7.49 ± 0.40 nmol min^{-1} mg^{-1}, and 5.55 ± 0.82 U mg^{-1} protein, respectively. This corresponded to inhibition rates of 72.09%, 38.71%, and 42.96% compared to the control group.

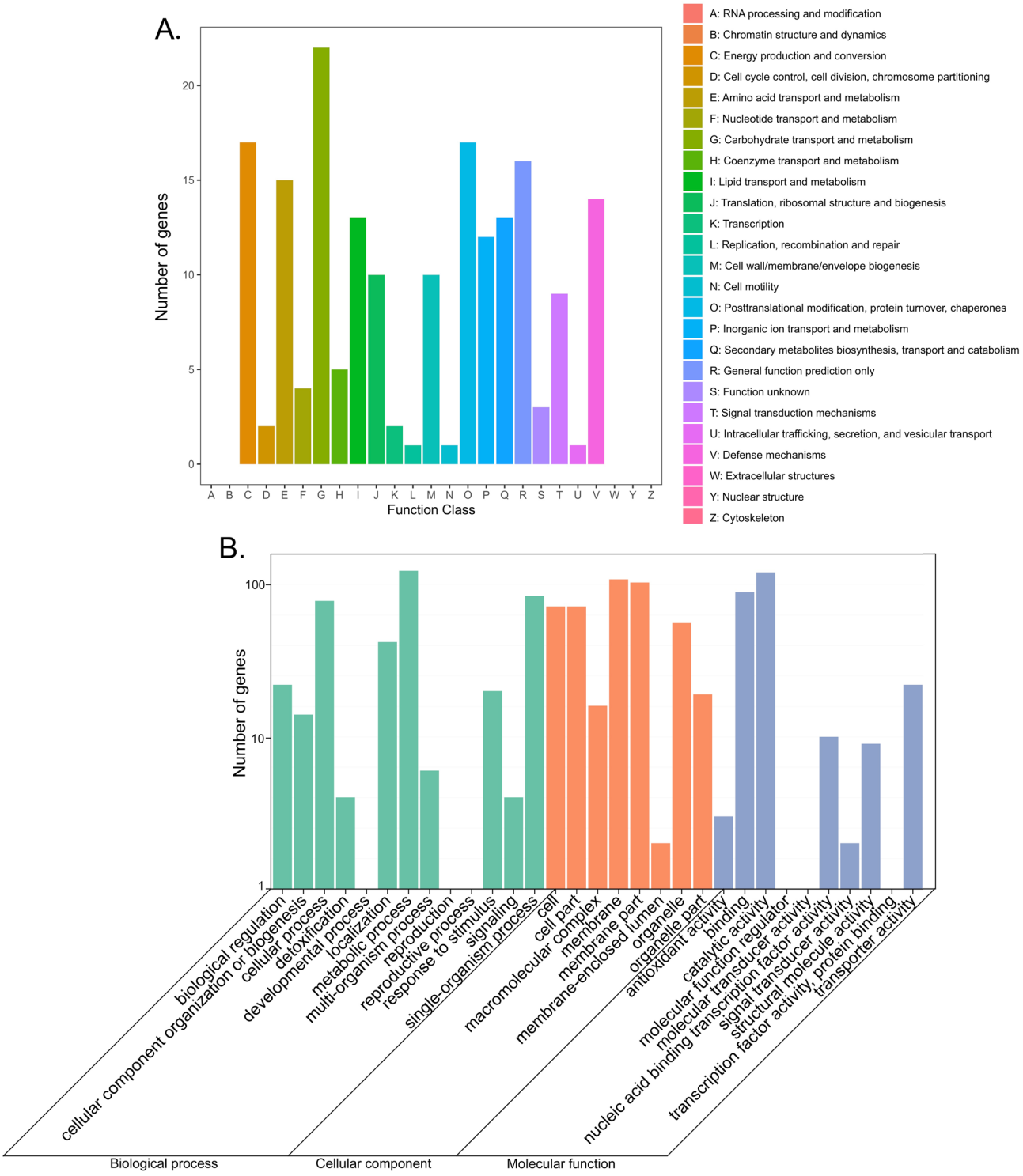

Fig. 2. (**A**) Cluster of orthologous groups classification of DEGs in *T. rubrum* affected by HQD. The x-axis indicates 25 functional COG categories. (**B**) GO analysis of DEGs in *T. rubrum* in response to HQD. The y-axis is shown in log10-scale.

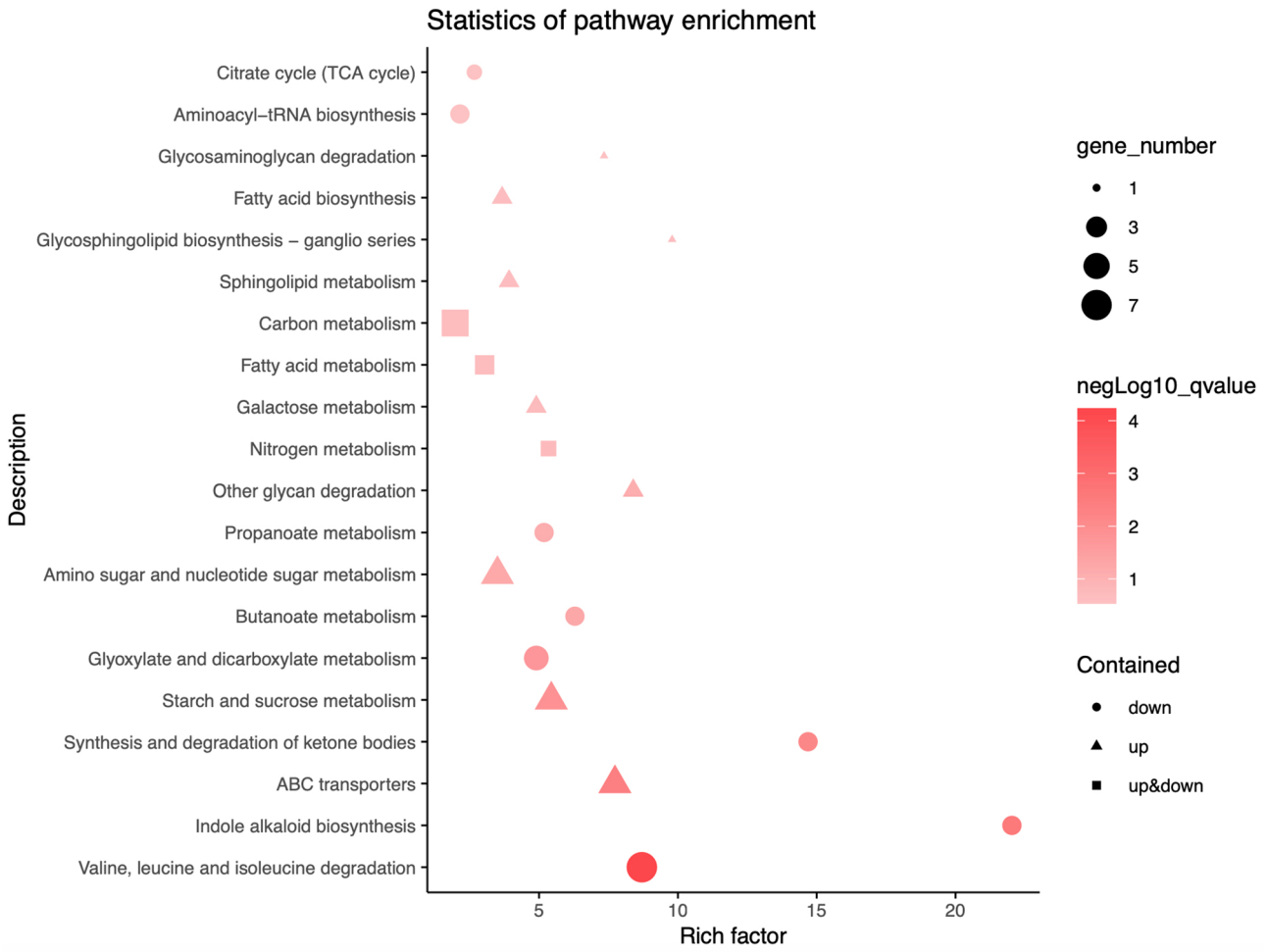

Fig. 3. The top 20 KEGG pathways enriched by DEGs in *T. rubrum* affected by HQD. The greater the rich factor, the higher the degree of enrichment. Pathways with a *q*-value smaller than 0.05 are assigned significantly enriched.

Table 4 summarizes our main findings in an attempt to correlate the expression levels of genes involved in the glyoxylate cycle obtained by RNA sequencing with those obtained by qRT-PCR, as well as with the corresponding enzyme activities, in *T. rubrum* strains treated with or without HQD.

Discussion

T. rubrum is the primary pathogenic fungus that can adapt to invade keratinized tissues such as skin, hair, and nails, and thus cause a wide spectrum of diseases medically known as dermatophytosis[51], tinea[52], or onychomycosis[53]. Current clinical drugs commonly used to treat infections caused by *T. rubrum* are often limited by the prolonged treatment duration, insufficient efficacy, antifungal resistance, and side effects. HQD, a classical TCM formulation, presents a promising alternative with its documented broad-spectrum antifungal activity, low incidence of drug resistance, and favorable safety profile[15]. In the present study, we preliminarily elucidate the mode of action of HQD against *T. rubrum* as a whole by integrating transcriptome sequencing validated by qRT-PCR and enzymatic activity assays. The findings suggested that the mode of action of HQD against *T. rubrum* may be related to the interference of the energy metabolism in *T. rubrum*, with citrate synthase emerging as a potential target of HQD.

Pathways related to energy metabolism contribute to metabolic flexibility, permitting microbial cells to survive in a nutrient-limited host environment during infection. During infection, *T. rubrum* specifically infects epidermal structures rich in keratin and lipids[54]. Under the glucose-limited conditions, fungal metabolism relies on carbon acquisition from the alternative nutritional sources[55–57], which are metabolized to the central metabolite acetyl-CoA to fuel the glyoxylate cycle and downstream gluconeogenesis for energy and glucose production[58]. Amino acid metabolism, particularly the degradation of branched-chain amino acids (e.g., valine, leucine, and isoleucine), served as a major pathway to produce acetyl-CoA in fungi[59]. The glyoxylate cycle bypasses two decarboxylation steps in the tricarboxylic acid (TCA) cycle, thereby permitting the net conversion of compounds with two-carbon atoms (especially acetyl-CoA) to metabolic intermediates that can be utilized to generate glucose[60–62].

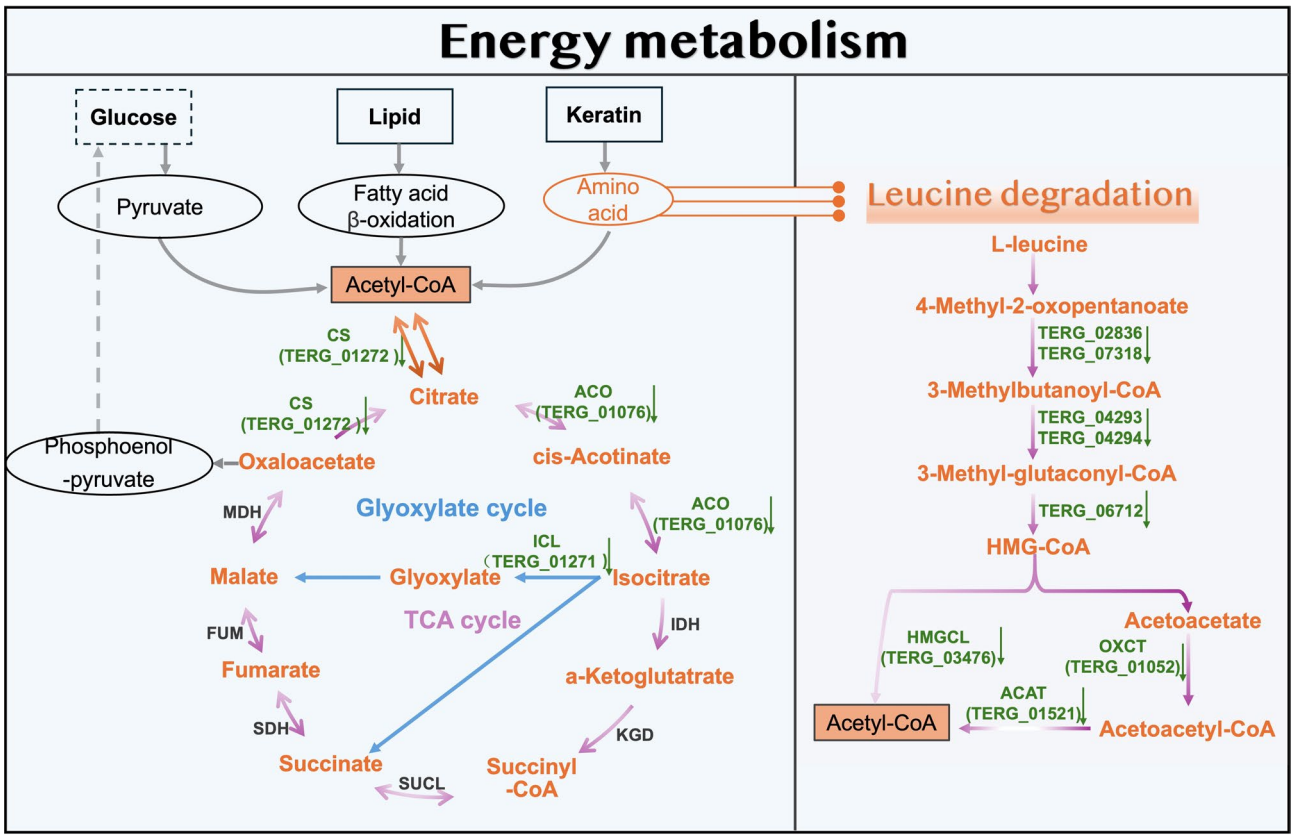

Fig. 4. DEGs in *T. rubrum* related to energy metabolism affected by HQD. Substances in the boxes drawn with a solid line represent the nutrients acquired from the host, while those in the box drawn with a dashed line represent glucose generated from other carbon sources. The DEGs marked with arrows were genes affected by HQD. The figure was based on the pathway maps of map00280, map00630 and map00020 in the KEGG database[48] (www.kegg.jp/kegg/kegg1.html).

Gene ID	Gene Product	Involved KEGG pathway	GO Function	Log2 (Fold Change)
TERG_01272	Citrate synthase (CS)	2-Oxocarboxylic acid metabolism Biosynthesis of amino acids Carbon metabolism Citrate cycle (TCA cycle) Glyoxylate and dicarboxylate metabolism	Citrate synthase activity	−1.4884
TERG_01076	Aconitate hydratase (ACO)	2-Oxocarboxylic acid metabolism Biosynthesis of amino acids Carbon metabolism Citrate cycle (TCA cycle) Glyoxylate and dicarboxylate metabolism	Hydro-lyase activity Cation binding DNA binding Iron-sulfur cluster binding	−1.1268
TERG_01271	Isocitrate lyase (ICL)	Carbon metabolism Glyoxylate and dicarboxylate metabolism	Oxo-acid-lyase activity	−1.1307
TERG_07318	Dihydrolipoyl transacylase (DBT)	Propanoate metabolism Valine, leucine and isoleucine degradation	Transferase activity	−1.6583
TERG_01052	3-oxoacid CoA-transferase (OXCT)	Butanoate metabolism Synthesis and degradation of ketone bodies Valine, leucine and isoleucine degradation	CoA-transferase activity	−1.3529
TERG_03476	Hydroxymethylglutaryl-CoA lyase (HMGCL)	Butanoate metabolism Peroxisome Synthesis and degradation of ketone bodies Valine, leucine and isoleucine degradation	Oxo-acid-lyase activity	−1.1204

Table 3. Information on DEGs in response to HQD identified by qRT-PCR assay.

Transcriptional analyses of *T. rubrum* revealed the extensive metabolic reprogramming in response to different growth conditions. When grown on proteins (keratin-soy media[63], powdered keratin[64], and powdered ox hull keratin[65], when co-cultured with human keratinocytes[66], or when exposed to a sublethal dose of cytotoxic drugs[55] and antifungal agents[33], key enzymes of the glyoxylate cycle in *T. rubrum* demonstrated to

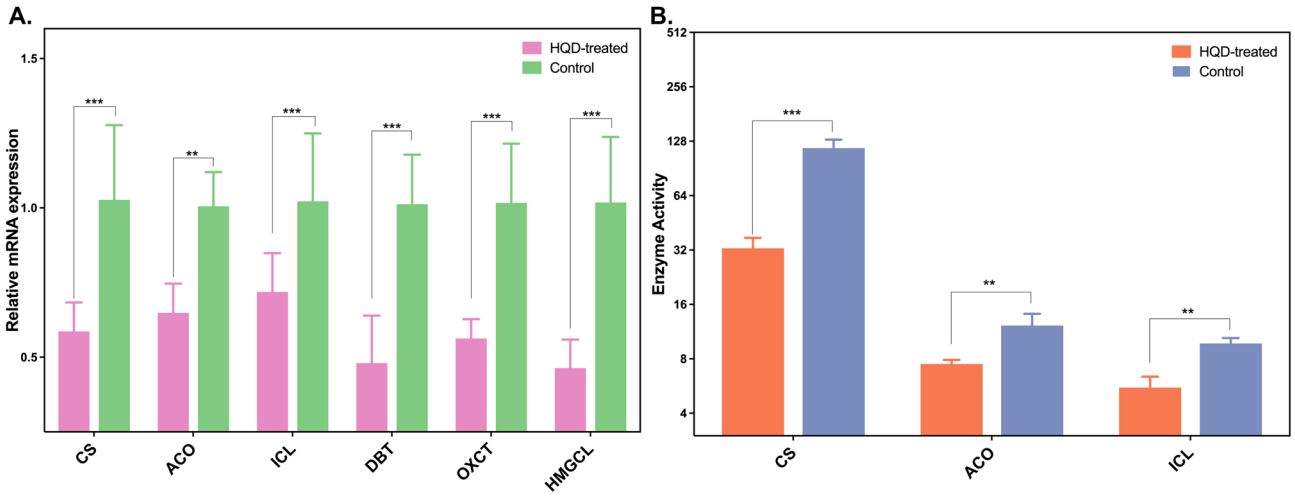

Fig. 5. (**A**) Relative gene expression levels of six DEGs identified by qRT-PCR. (**B**) Effect of HQD on the activities of ACO, CS, and ICL in *T. rubrum*. The activities of ICL and CS are expressed as U mg-1 protein, and that of ACO is shown as nmol min-1 mg-1 protein. The y-axis is shown in log2-scale. In each sub-figure, the bars represent the standard deviations of the data. Statistical significance was determined by: ** indicates p-value < 0.01; *** indicates p-value < 0.001.

Gene ID	Gene Product	Group	Log2 (Fold Change) *	Relative mRNA Expression #	Enzymatic Activity ¥
TERG_01272	Citrate synthase	HQD-treatment	−1.4884	0.59 ± 0.10	32.75 ± 4.60
		control		1.03 ± 0.25	117.36 ± 13.29
TERG_01076	Aconitate hydratase	HQD-treatment	−1.1268	0.65 ± 0.10	7.49 ± 0.40
		control		1.01 ± 0.11	12.22 ± 1.98
TERG_01271	Isocitrate lyase	HQD-treatment	−1.1307	0.72 ± 0.13	5.55 ± 0.82
		control		1.02 ± 0.23	9.73 ± 0.70

Table 4. Gene expression, relative mRNA expression and enzymatic activity of genes of the glyoxylate cycle in strains with or without HQD treatment. * Fold change values of HQD-treatment samples compared with the control samples obtained by transcriptome sequencing. # Relative mRNA expression values obtained by qRT-PCR. ¥ The activities of ICL and CS were expressed as U mg^{-1} protein, and that of ACO was shown as nmol min^{-1} mg^{-1} protein.

be highly active. This adaptive change highlights the glyoxylate cycle as a potential pathway for antifungal drug development[61].

Notably, the glyoxylate cycle, a fungal primary metabolic process, is absent in humans. Among the metabolic enzymes involved in this cycle, ICL is an exclusive and essential component of this metabolic route. The relation between enzyme ICL and the virulence of various fungi has been well established in species such as *Candida albicans*[67], *Candida glabrata*[68], and Budding Yeast[69]. For instance, *C. albicans* mutant strains lacking the gene encoding ICL exhibit reduced virulence in a mouse model[70]. Similarly, disruption of the ICL1 gene in *C. glabrata* conferred a severe attenuation of virulence in a murine model of invasive candidiasis[68]. Building on these findings, we hypothesize that ICL may serve as a potential antifungal target of HQD against *T. rubrum*. The precise role of ICL in the metabolic flexibility and virulence of *T. rubrum* will be fully elucidated in our subsequent studies using gene knock-out experiments.

Given the abundance of novel scaffolds inherent in natural products derived from the TCM formulas, the systematic analysis of individual components of the HQD offers valuable insights for the development of new small-molecule antifungal agents. Comprehensive information on the chemical constituents of HQD can be retrieved from public databases, including TCMSID[71], ETCM v2.0[72], and TCMbank[73]. Beyond these herbal repositories, the current scientific knowledge regarding the composition of HQD has been documented in reference[74]. As outlined in the Introduction section, several ingredients — including baicalin[22], baicalein[23], and wogonin[23] — have been demonstrated to exert antifungal activity and thus hold potential as potent antifungal agents. These three compounds have been reported to exhibit antifungal activity, but their efficacy against *T. rubrum* has not yet been confirmed. We hope the findings will facilitate relevant research by other scientists.

Conclusion

In summary, our study integrated transcriptome sequencing, qRT-PCR, and enzyme activity assays to elucidate the antifungal mechanism of HQD against *T. rubrum*. The majority of the expression-changed genes were identified as being involved in energy metabolism. The expression levels of genes and the enzymatic activities of three enzymes involved in the glyoxylate cycle were dramatically changed upon HQD treatment, highlighting their crucial roles in the antifungal activity. Our study provided the first comprehensive exploration of the mechanisms involved in the exposure of *T. rubrum* to HQD. The potential of HQD as a therapeutic intervention against dermatophytes was confirmed. Future research should focus on the biological validation of HQD targeting the ICL of *T. rubrum* by using knock-out methods.

Data availability

The transcriptome sequencing data have been deposited in the GEO database under the accession number GSE300994. For further details, please visit the GEO Accession viewer at https://www.ncbi.nlm.nih.gov/geo/query/acc.cgi? acc=GSE300994.

Received: 26 August 2025; Accepted: 29 December 2025
Published online: 07 January 2026

References

1. Whittle, S. B., Williamson, K. C. & Russell, H. V. Incidence and risk factors of bacterial and fungal infection during induction chemotherapy for high-risk neuroblastoma. *Pediatr. Hematol. Oncol.* **34** (5), 331–342 (2017).
2. Sun, Y. et al. Invasive fungal infection in patients receiving chemotherapy for hematological malignancy: a multicenter, prospective, observational study in China. *Tumor Biology*. **36**, 757–767 (2015).
3. Rouzaud, C. et al. Severe dermatophytosis in solid organ transplant recipients: a French retrospective series and literature review. *Transpl. Infect. Disease*. **20** (1), e12799 (2018).
4. de Oliveira Pereira, F., Gomes, S. M., Lima da Silva, S., Paula de Castro Teixeira, A. & Lima, I. O. The prevalence of dermatophytoses in brazil: a systematic review. *J. Med. Microbiol.* **70** (3), 001321 (2021).
5. Chanyachailert, P., Leeyaphan, C. & Bunyaratavej, S. Cutaneous fungal infections caused by dermatophytes and Non-Dermatophytes: an updated comprehensive review of epidemiology, clinical Presentations, and diagnostic testing. *J. Fungi (Basel).* **9**(6), 669 (2023).
6. Nweze, E. I. & Eke, I. E. Dermatophytes and dermatophytosis in the Eastern and Southern parts of Africa. *Med. Mycol.* **56** (1), 13–28 (2018).
7. Verma, S. B. et al. The unprecedented epidemic-like scenario of dermatophytosis in india: I. Epidemiology, risk factors and clinical features. *Indian J. Dermatol. Venereol. Leprol.* **87** (2), 154–175 (2021).
8. Mularoni, A., Graziano, E. & Todaro, F. Invasive trichophyton infection in a liver transplant recipient. *Transpl. Infect. Dis.* **24** (2), e13794 (2022).
9. Ansai, O. et al. Deep dermatophytosis caused by trichophyton rubrum in an elderly patient with CARD9 deficiency: A case report and literature review. *J. Dermatol.* **51** (2), 294–300 (2024).
10. Ridzuan, P. M. et al. Mini review on dermatomycosis. *J. Sci. Math. Lett.* **8** (1), 6–15 (2020).
11. Ben-Ami, R. & Kontoyiannis, D. P. Resistance to antifungal drugs. *Infect. Disease Clin.* **35** (2), 279–311 (2021).
12. Perlin, D. S., Rautemaa-Richardson, R. & Alastruey-Izquierdo, A. The global problem of antifungal resistance: prevalence, mechanisms, and management. *Lancet. Infect. Dis.* **17** (12), e383–e92 (2017).
13. Liu, Q. et al. Antifungal activity in plants from Chinese traditional and folk medicine. *J. Ethnopharmacol.* **143** (3), 772–778 (2012).
14. Lopes, G., Pinto, E. & Salgueiro, L. Natural products: an alternative to conventional therapy for dermatophytosis? *Mycopathologia* **182**, 143–167 (2017).
15. Wei, Z. et al. Traditional Chinese medicine has great potential as candidate drugs for lung cancer: A review. *J. Ethnopharmacol.* **300**, 115748 (2023).
16. Li, M. et al. Anti-inflammatory effects of Huangqin Decoction on dextran sulfate sodium-induced ulcerative colitis in mice through regulation of the gut microbiota and suppression of the Ras-PI3K-Akt-HIF-1α and NF-κB pathways. *Front. Pharmacol.* **10**, 1552 (2020).
17. Yan, B-F. et al. Huangqin Decoction mitigates hepatic inflammation in high-fat diet-challenged rats by inhibiting TLR4/NF-κB/NLRP3 pathway. *J. Ethnopharmacol.* **303**, 115999 (2023).
18. Yan, M., Zuo, F., Song, H., Ye, W-H. & Zhou, Z. -m. Comparative study on antibacterial effects of huangqin-tang and its metabolites produced by intestinal flora. *Zhongguo Zhong Yao Za Zhi*. **28** (3), 243–246 (2003).
19. Zhou, Y. X., Gong, X. H., Zhang, H. & Peng, C. A review on the pharmacokinetics of Paeoniflorin and its anti-inflammatory and Immunomodulatory effects. *Biomed. Pharmacother.* **130**, 110505 (2020).
20. Zhao, Z. et al. Glycyrrhizic acid nanoparticles as antiviral and Anti-inflammatory agents for COVID-19 treatment. *ACS Appl. Mater. Interfaces*. **13** (18), 20995–21006 (2021).
21. Messier, C. & Grenier, D. Effect of licorice compounds licochalcone A, glabridin and glycyrrhizic acid on growth and virulence properties of Candida albicans. *Mycoses* **54** (6), e801–e806 (2011).
22. Wang, T. et al. In vitro antifungal activity of Baicalin against Candida albicans biofilms via apoptotic induction. *Microb. Pathog.* **87**, 21–29 (2015).
23. Da, X. et al. Antifungal activity and mechanism of action of Ou-gon (Scutellaria root extract) components against pathogenic fungi. *Sci. Rep.* **9** (1), 1683 (2019).
24. Shen, C. et al. Antifungal activity and potential mechanism of action of Huangqin Decoction against trichophyton rubrum. *J. Med. Microbiol.* **73**(2). https://doi.org/10.1099/jmm.0.001805 (2024).
25. Costa, V., Angelini, C., De Feis, I. & Ciccodicola, A. Uncovering the complexity of transcriptomes with RNA-Seq. *Biomed. Res. Int.* **2010** (1), 853916 (2010).
26. Lockhart, D. J. & Winzeler, E. A. Genomics, gene expression and DNA arrays. *Nature* **405** (6788), 827–836 (2000).
27. Wang, Z., Gerstein, M. & Snyder, M. RNA-Seq: a revolutionary tool for transcriptomics. *Nat. Rev. Genet.* **10** (1), 57–63 (2009).
28. Li, Z., Qi, F. & Li, F. Establishment of a gene signature to predict prognosis for patients with lung adenocarcinoma. *Int. J. Mol. Sci.* **21** (22), 8479 (2020).
29. Xiao, C. et al. Digital gene expression analysis of microsporum canis exposed to Berberine chloride. *PloS One*. **10** (4), e0124265 (2015).
30. Li, M., Chen, L., Zhao, Y., Sun, H. & Zhao, L. Research on the mechanism of HRP relieving IPEC-J2 cells immunological stress based on transcriptome sequencing analysis. *Front. Nutr.* **9**, 944390 (2022).

31. Hovhannisyan, H. & Gabaldón, T. Transcriptome sequencing approaches to elucidate Host-Microbe interactions in opportunistic human fungal pathogens. *Curr. Top. Microbiol. Immunol.* **422**, 193–235 (2019).
32. Shentu, X. P. et al. Transcriptome sequencing and gene expression analysis of trichoderma Brevicompactum under different culture conditions. *PLoS One*. **9** (4), e94203 (2014).
33. Komoto, T. T. et al. Gene expression response of trichophyton rubrum during coculture on keratinocytes exposed to antifungal agents. *Evidence-based Complement. Altern. Med.* **2015**, 180535 (2015).
34. Wang, M. et al. Transcriptome sequencing revealed the inhibitory mechanism of ketoconazole on clinical microsporum canis. *J. Vet. Sci.* **22**(1), e4 (2021).
35. Wacker, S. A., Houghtaling, B. R., Elemento, O. & Kapoor, T. M. Using transcriptome sequencing to identify mechanisms of drug action and resistance. *Nat. Chem. Biol.* **8** (3), 235–237 (2012).
36. Yang, S. Q., Ge, Y. J. & Shen, C. Y. Disclosing antifungal activity of Huangqin Decoction upon trichophyton mentagrophytes and exploring its potential inhibitory mechanisms through transcriptome sequencing and qRT-PCR. *Sci. Rep.* **15** (1), 13321 (2025).
37. Chen, J., Blechert, O., Xiong, S. & Zhan, P. Differential deuterolysin expression with a peak at low pH in human pathogenic fungi *Trichophyton rubrum* and *T. mentagrophytes*. *Med. Mycol.* **61**(4), myad034 (2023).
38. Li, R., Li, Y., Kristiansen, K. & Wang, J. SOAP: short oligonucleotide alignment program. *Bioinformatics* **24** (5), 713–714 (2008).
39. Kim, D., Langmead, B. & Salzberg, S. L. HISAT: a fast spliced aligner with low memory requirements. *Nat. Methods*. **12** (4), 357–360 (2015).
40. Clough, E. & Barrett, T. The gene expression omnibus database. *Methods Mol. Biol.* **1418**, 93–110 (2016).
41. Pertea, M. et al. StringTie enables improved reconstruction of a transcriptome from RNA-seq reads. *Nat. Biotechnol.* **33** (3), 290–295 (2015).
42. Love, M. et al. Package 'DESeq2'. (2018).
43. Benjamini, Y. & Yekutieli, D. The control of the false discovery rate in multiple testing under dependency. *Ann. Stat.* **29**(4), 1165–1188 (2001).
44. Tatusov, R. L. et al. The COG database: new developments in phylogenetic classification of proteins from complete genomes. *Nucleic Acids Res.* **29** (1), 22–28 (2001).
45. Gene Ontology, C. The gene ontology (GO) database and informatics resource. *Nucleic Acids Res.* **32** (suppl_1), D258–D61 (2004).
46. Aoki, K. F. & Kanehisa, M. Using the KEGG database resource. *Curr. Protocols Bioinf.* **11** (1), 1 (2005).
47. Aoki-Kinoshita, K. F. & Kanehisa, M. Gene annotation and pathway mapping in KEGG. *Comp. Genomics.* **396**, 71–91 (2007).
48. Kanehisa, M., Furumichi, M., Sato, Y., Matsuura, Y. & Ishiguro-Watanabe, M. KEGG: biological systems database as a model of the real world. *Nucleic Acids Res.* **53** (D1), D672–d7 (2025).
49. Wu, J., Mao, X., Cai, T., Luo, J. & Wei, L. KOBAS server: a web-based platform for automated annotation and pathway identification. *Nucleic Acids Res.* **34** (suppl_2), W720–W4 (2006).
50. Livak, K. J. & Schmittgen, T. D. Analysis of relative gene expression data using real-time quantitative PCR and the 2− ΔΔCT method. *Methods* **25** (4), 402–408 (2001).
51. Begum, J., Mir, N. A., Lingaraju, M. C., Buyamayum, B. & Dev, K. Recent advances in the diagnosis of dermatophytosis. *J. Basic. Microbiol.* **60** (4), 293–303 (2020).
52. Leung, A. K. C., Leong, K. F. & Lam, J. M. Tinea imbricata: an overview. *Curr. Pediatr. Rev.* **15** (3), 170–174 (2019).
53. Leung, A. K. C. et al. Onychomycosis: an updated review. *Recent. Pat. Inflamm. Allergy Drug Discov*. **14** (1), 32–45 (2020).
54. Weitzman, I. & Summerbell, R. C. The dermatophytes. *Clin. Microbiol. Rev.* **8** (2), 240–259 (1995).
55. Persinoti, G. F. et al. RNA-sequencing analysis of trichophyton rubrum transcriptome in response to sublethal doses of acriflavine. *BMC Genom.* **15** (Suppl 7(Suppl 7), S1 (2014).
56. Mohammadifard, H., Amini, K., Bayat, M., Hashemi, S. J. & Noorbakhsh, F. Molecular study and antifungal susceptibility profile of trichophyton rubrum and trichophyton mentagrophytes strains isolated from lesions of humans and cattle. *Iran. J. Microbiol.* **14** (4), 587–597 (2022).
57. Chen, J., Gao, Y., Xiong, S., Peng, Z. & Zhan, P. Expression profiles of protease in onychomycosis-related pathogenic trichophyton rubrum and Tinea capitis-related pathogenic trichophyton violaceum. *Mycopathologia* **189** (1), 14 (2024).
58. Chew, S. Y., Chee, W. J. Y. & Than, L. T. L. The glyoxylate cycle and alternative carbon metabolism as metabolic adaptation strategies of Candida glabrata: perspectives from Candida albicans and Saccharomyces cerevisiae. *J. Biomed. Sci.* **26** (1), 52 (2019).
59. Vorapreeda, T., Thammarongtham, C., Cheevadhanarak, S. & Laoteng, K. Alternative routes of acetyl-CoA synthesis identified by comparative genomic analysis: involvement in the lipid production of oleaginous yeast and fungi. *Microbiol. (Reading)*. **158** (Pt 1), 217–228 (2012).
60. Cronan, J. E. Jr. & Laporte, D. Tricarboxylic acid cycle and glyoxylate bypass. *EcoSal Plus.* **1**(2). https://doi.org/10.1128/ecosalplus.3.5.2 (2005).
61. Huang, Z. et al. The methylcitrate cycle and its crosstalk with the glyoxylate cycle and Tricarboxylic acid cycle in pathogenic fungi. *Molecules* **28**(18), 6667 (2023).
62. Fleck, C. B., Schobel, F. & Brock, M. Nutrient acquisition by pathogenic fungi: nutrient availability, pathway regulation, and differences in substrate utilization. *Int. J. Med. Microbiol.* **301** (5), 400–407 (2011).
63. Zaugg, C. et al. Gene expression profiling in the human pathogenic dermatophyte trichophyton rubrum during growth on proteins. *Eukaryot. Cell.* **8** (2), 241–250 (2009).
64. Peres, N. T. et al. In vitro and ex vivo infection models help assess the molecular aspects of the interaction of trichophyton rubrum with the host milieu. *Med. Mycol.* **54** (4), 420–427 (2016).
65. Martins, M. P., Rossi, A., Sanches, P. R., Bortolossi, J. C. & Martinez-Rossi, N. M. Comprehensive analysis of the dermatophyte trichophyton rubrum transcriptional profile reveals dynamic metabolic modulation. *Biochem. J.* **477** (5), 873–885 (2020).
66. Petrucelli, M. F. et al. The transcription factor StuA regulates the glyoxylate cycle in the dermatophyte trichophyton rubrum under carbon starvation. *Int. J. Mol. Sci.* **25**(1), 405 (2023).
67. Ishola, O. A. et al. The role of isocitrate lyase (ICL1) in the metabolic adaptation of Candida albicans biofilms. *Jundishapur J. Microbiol.* **9** (9), e38031 (2016).
68. Chew, S. Y. et al. Glyoxylate cycle gene ICL1 is essential for the metabolic flexibility and virulence of Candida glabrata. *Sci. Rep.* **9** (1), 2843 (2019).
69. Kwon, Y. Y., Lee, H. J., Lee, M. J., Lee, Y. S. & Lee, C. K. The ICL1 and MLS1 genes, integral to the glyoxylate cycle, are essential and specific for caloric restriction-mediated extension of lifespan in budding yeast. *Adv. Biology*. **8** (9), e2400083 (2024).
70. Lorenz, M. C. & Fink, G. R. Life and death in a macrophage: role of the glyoxylate cycle in virulence. *Eukaryot. Cell*. **1** (5), 657–662 (2002).
71. Zhang, L. X. et al. TCMSID: a simplified integrated database for drug discovery from traditional Chinese medicine. *J. Cheminform.* **14** (1), 89 (2022).
72. Zhang, Y. et al. ETCM v2.0: an update with comprehensive resource and rich annotations for traditional Chinese medicine. *Acta Pharm. Sin B*. **13** (6), 2559–2571 (2023).
73. Lv, Q. et al. TCMBank: bridges between the largest herbal medicines, chemical ingredients, target proteins, and associated diseases with intelligence text mining. *Chem. Sci.* **14** (39), 10684–10701 (2023).
74. Zhuo-ran, S., Dan, J., Xiao-fei, C. & Yi-feng, C. Identification on components of Huangqin Tang and rats blood components after administration based on UHPLC-QTOF MS analysis. *J. Instrumental Anal.* **42** (8), 960–967 (2023).

Acknowledgements
This study was financially supported by the Natural Science Foundation of Jiangxi Province (No. 20232BAB216124) and the Jiangxi Provincial Health Technology Project (No. 202610204). The funders had no role in study design, data collection and analysis, decision to publish, or preparation of the manuscript.

Author contributions
Y.S.: Data curation, Methodology, Writing-original draft, Writing-review & editing; H.Y.: Data curation, Investigation, Writing-review & editing; G.Y.: Investigation, Methodology, Writing-review & editing; S.B.: Supervision, Writing-review & editing; S.C.: Funding acquisition, Investigation, Methodology, Writing-review & editing.

Funding
This study was financially supported by the Natural Science Foundation of Jiangxi Province (No. 20232BAB216124) and the Jiangxi Provincial Health Technology Project (No. 202610204).

Declarations

Competing interests
The authors declare no competing interests.

Additional information
Supplementary Information The online version contains supplementary material available at https://doi.org/10.1038/s41598-025-34456-8.

Correspondence and requests for materials should be addressed to C.S.

Reprints and permissions information is available at www.nature.com/reprints.

Publisher's note Springer Nature remains neutral with regard to jurisdictional claims in published maps and institutional affiliations.